EPRG-PRCI-APGA
23rd Joint Technical Meeting
Edinburgh, Scotland
6–10 June 2022

EVALUATION OF REMAINING BURST STRENGTH PREDICTION MODELS FOR DOWNHOLE CASING
PAPER NUMBER: 33

Gang Tao*
C-FER Technologies (1999) Inc., Edmonton AB, Canada

Andrew Lloyd
Enterprise Products, Houston, TX, USA

* presenting author

ABSTRACT

Determination of remaining burst strength capacity of corroded casing is one of the most critical tasks in well integrity management. The current industry practice involves measurement of corrosion-induced metal-loss in casing strings using various downhole logging tools. The measured metal-loss geometries are then used in various semi-empirical models to estimate the remaining burst capacity. Although these remaining burst strength prediction models have been previously calibrated through extensive physical burst tests on line pipe samples, their prediction accuracy for downhole casing remains unclear.

A study of remaining burst strength of corroded casing was conducted as part of a comprehensive research program for underground gas storage sponsored by the Pipeline Research Council International, Inc. and the US Department of Transportation's Pipeline and Hazardous Materials Safety Administration. Full-scale burst tests and advanced finite element analysis (FEA) were conducted on casing specimens with metal-loss features. A variety of remaining burst strength prediction models were benchmarked based on the test results. The failure mechanism and the effects of in-situ axial constraint (i.e., for cemented casing) on the burst strength of corroded casing were investigated using FEA. The outcome of this study provided valuable insights into the prediction capability of various remaining burst strength models and established a comprehensive knowledge base for further development of these models for downhole casing applications.

Keywords: Casing Corrosion, Remaining Burst Strength, Full-scale Test, Finite Element Analysis, Model Benchmark

DISCLAIMER

This work was funded in part, under the Department of Transportation, Pipeline and Hazardous Materials Safety Administration. The views and conclusions contained in this document are those of the authors and should not be interpreted as representing the official policies, either expressed or implied, of the Pipeline and Hazardous Materials Safety Administration, the Department of Transportation, or the U.S. Government.

1. INTRODUCTION

Mechanical damage or corrosion-induced metal-loss poses a significant threat to downhole casing integrity, especially for underground gas storage (UGS) wells that are designed to have decades of operating life. Safe operation of UGS wells requires periodic inspection of casing condition using various downhole logging tools to properly identify and size metal-loss anomalies. These inspection data are used to estimate the remaining burst strength using various methods. However, the calculated remaining burst strength can have significant uncertainties due to the variations of the input parameters used with this process. For example, the measurement accuracy of metal-loss feature size and depth from the inspection, variability in the casing material properties, unknown in-situ load conditions, and the prediction model error would all contribute to the uncertainties of the estimated remaining burst strength. Due to the lack of study in these areas, these uncertainties remain unclear to UGS operators.

A series of comprehensive research programs have been sponsored in recent years through the Pipeline Research Council International (PRCI) and US Department of Transportation's Pipeline and Hazardous Materials Safety Administration (PHMSA) in an effort to address the knowledge gaps in casing corrosion management. In 2019, a comprehensive laboratory test program was completed to assess casing corrosion logging tool performance, sponsored by the Underground Storage Technical Committee (USTC) of PRCI [1]. This program evaluated the performance of several casing corrosion logging techniques, including multi-finger caliper, ultrasonic testing, magnetic flux leakage, magnetic eddy current, and electromagnetic techniques. Upon completion of the PRCI casing logging tool test program, a multiphase research program on the evaluation of casing integrity for UGS wells was initiated by PRCI and PHMSA [2]. This program expanded the laboratory evaluation of casing corrosion logging tools that demonstrated the overall best performance among technologies evaluated in the preceding PRCI test program. In addition, this program included a comprehensive study of remaining burst strength of corroded casing and the development of a reliability-based casing corrosion management framework. The PRCI/PHMSA co-sponsored program was completed in 2021. This paper highlights the work conducted in this program to evaluate the remaining burst strength prediction models.

The previous research effort developed and calibrated remaining burst strength prediction models for corroded line pipe specimens based on a large number of physical burst tests [3]. Validation of these models through testing of corroded downhole casing specimens is limited [4,5,6]. Since the majority of these models are semi-empirical and do not fully capture the fundamental mechanical response of the metal-loss anomalies, their prediction accuracy for downhole casing remains unclear. This motivated the investigation of the prediction capability of the existing remaining burst strength prediction models for downhole casing applications, combining full-scale burst tests and advanced finite element analysis (FEA). The failure mechanism and the effects of in-situ locked-in axial loads (i.e., for cemented casing) on the remaining burst strength of corroded casing were also investigated.

2. PHYSICAL LABORATORY TEST

In this study, three casing configurations (listed in Table 1) that represent the most popular casing strings in depleted reservoir UGS wells in the US were tested. The physical laboratory tests included both coupon tensile tests and full-scale burst tests.

Outside Diameter	Weight	Wall Thickness	Diameter to Thickness (D/t) Ratio	Grade
114.3 mm (4.5 in)	17.26 kg/m (11.6 lb/ft)	6.35 mm (0.25 in)	18.0	J55
139.7 mm (5.5 in)	23.07 kg/m (15.5 lb/ft)	6.99 mm (0.275 in)	20.0	J55
177.8 mm (7.0 in)	34.23 kg/m (23.0 lb/ft)	8.05 mm (0.317 in)	22.1	J55

Table 1 – Tested casing samples

2.1. Coupon Tensile Test

To accurately measure the stress-strain curve of the sample materials for FEA modeling, high-precision coupon tests were conducted following ASTM E111 specifications [7]. This test procedure was designed to measure the Young's modulus of the material using much stricter test control and measurement requirements than other test specifications, such as ASTM E370 [8] and ASTM E8 [9]. Key test specifications in the coupon tensile test included:

- Rectangular coupons with more than 80% of the original pipe wall thickness were used to capture the average through-thickness properties of the casing material;
- Double Class B-1 extensometers were placed on opposite sides of the coupon for simultaneous strain measurement, as shown in Figure 1;
- A strict alignment check following ASTM E111 specifications was followed; and
- Tests were conducted in strain-control mode at a constant strain rate of 0.3% per minute up to the ultimate tensile strength (UTS) point.

Figure 2 presents example stress-strain curves for the three casing samples and a close-up view of the stress-strain curves within the elastic-plastic transition region. The high-accuracy coupon test results clearly show that the J55 casing materials started to develop plastic deformation at approximately 276 MPa (40 ksi), which is often referred to as the proportional limit. Note that, as per the API 5CT specification [10], the API yield strength for J55 casing grade is defined as the stress value at 0.5% engineering strain. The key mechanical properties determined from the stress-strain curves are summarized in Table 2. All burst test specimens were prepared from the same pipe joint as the tensile test sample for each pipe configuration to ensure that the measured mechanical properties were representative of the burst specimens.

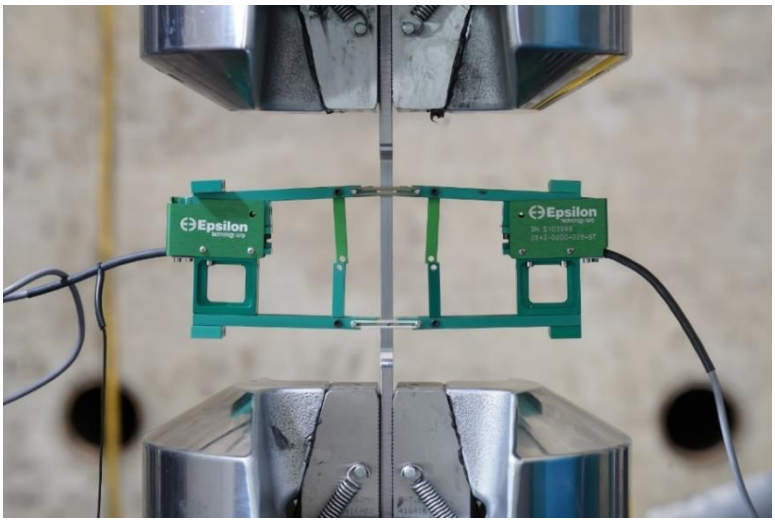

Figure 1 – Coupon tensile test setup

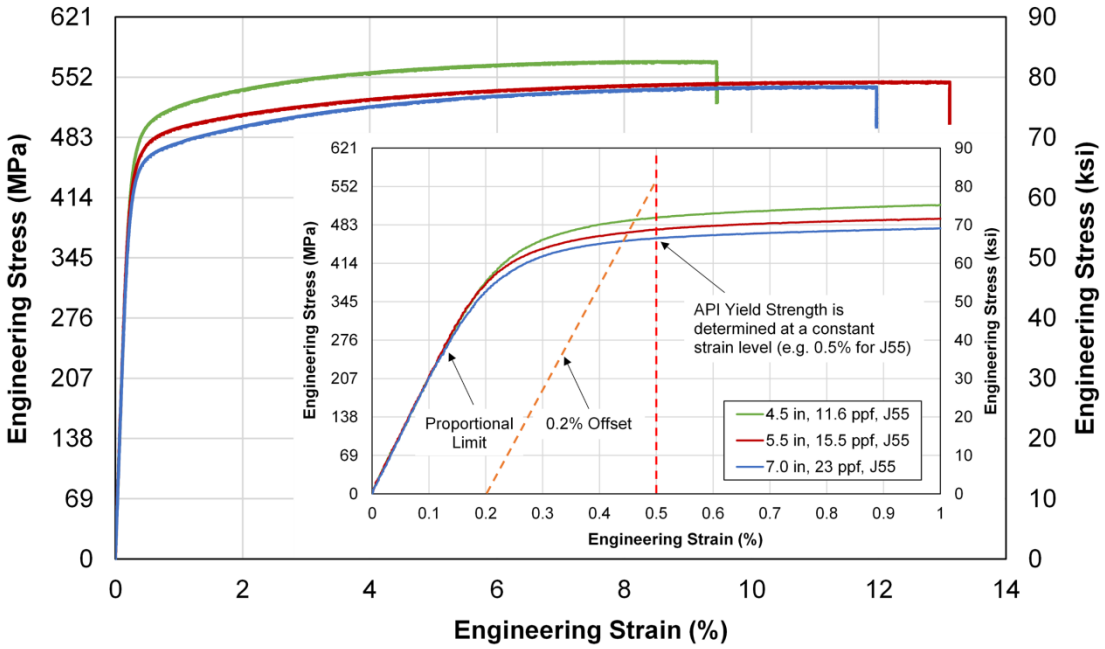

Figure 2 – High-accuracy stress-strain curves from ASTM E111 tensile tests

	114.3 mm, 17.26 kg/m (4.5 in, 11.6 lb/ft) J55	139.7 mm, 23.07 kg/m (5.5 in, 15.5 lb/ft) J55	177.8 mm, 34.23 kg/m (7.0 in, 23 lb/ft) J55
Young's Modulus	204 GPa (29,600 ksi)	204 GPa (29,600 ksi)	206 GPa (29,900 ksi)
API Yield Strength	495 MPa (71.8 ksi)	474 MPa (68.8 ksi)	459 MPa (66.5 ksi)
Tensile Strength	569 MPa (82.5 ksi)	546 MPa (79.2 ksi)	541 MPa (78.4 ksi)

Table 2 – Key mechanical properties of casing samples

In addition, the coupon tests included characterization of the time-dependent response of the casing material, which can have a significant impact on casing burst strength [11]. After reaching the UTS, the coupon was held at a constant strain level for one hour to capture the stress relaxation response, as shown in Figure 3. Most importantly, the test results show that the UTS values for two of the three coupons dropped below the specified minimum tensile strength (SMTS) of 517 MPa (75 ksi) for the J55 casing grade specified in API 5CT. Although the 114.3 mm (4.5 in) casing material sample remained above the SMTS after one hour, the downward trend suggests that the UTS could eventually drop below the SMTS. However, it's important to point out that such material behavior is not an indication of sub-standard casing products, since the UTS values exceed the SMTS following the tensile test procedure ASTM A370 [8] as specified by API 5CT. The stress relaxation response reflects the time dependency or strain-rate dependency of the casing material in its post-yield region [11]. In general, the material would show a reduction in post-yield strength as the strain rate in a tensile test decreases.

Many laboratory tests, including coupon tensile tests and burst tests, are typically conducted at relatively higher loading rates than what occurs in UGS wells, where tubulars are typically subjected to lower loading rates or sustained pressure. Therefore, laboratory tests following current testing standards tend to over-estimate the material strength and burst strength compared to the in-service casing performance in UGS wells.

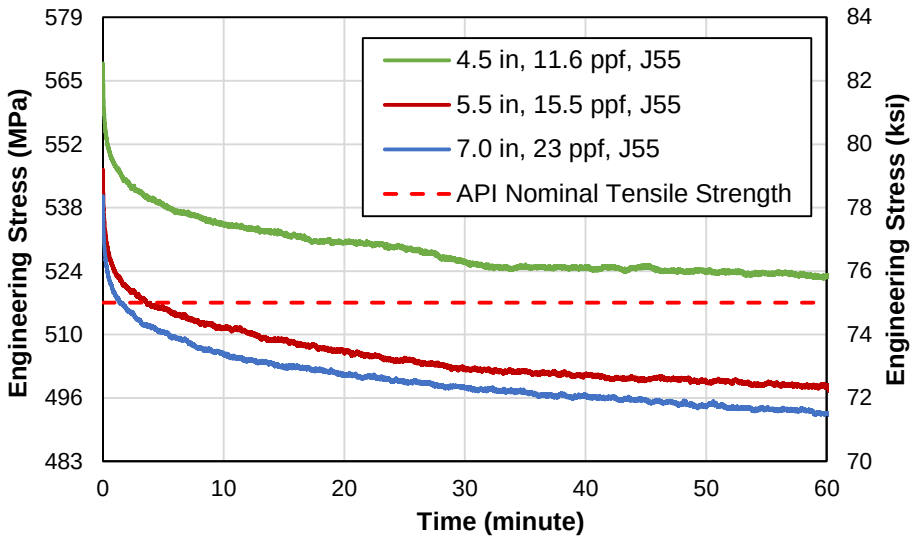

Figure 3 – Stress relaxation curves

2.2. Full-scale Burst Test

Twenty full-scale burst tests in total were conducted on the three casing samples. Each test specimen included an artificial metal-loss feature with a random profile at the center. Each metal-loss feature has an axial length and a circumferential width of a few inches, and a metal-loss depth of approximately 40% to 70% of the wall thickness. End caps were welded on both ends of each burst test specimen, as shown in Figure 4. The unconstrained section (between the end caps) had a length of approximately 1.2 to 1.5 m (greater than eight-times the pipe outer diameter), which ensures a negligible effect on the burst strength of the specimens. As per the burst test specification in API TR 5C3 Annex C [12], the pressure transducer was installed on the opposite end of the specimen from the pressure supply to minimize recording the pressure spikes related to the pump stroking during testing. The burst tests were executed within an isolated blast containment chamber. The specimen pressure was manually increased at a nominal rate of 1.38 MPa/minute (200 psi/minute) until specimen failure.

Figure 5 shows two different failure modes of the burst specimens: a ductile rupture and a small leak. The burst pressure results were used to benchmark the selected remaining burst strength prediction models.

Figure 4 – Capped-end burst test specimen

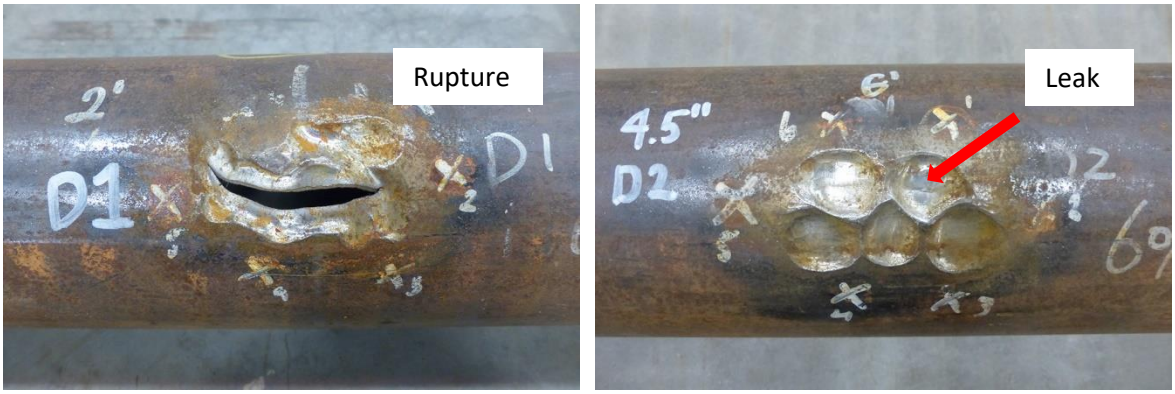

Figure 5 – Failed burst specimens

3. FINITE ELEMENT ANALYSIS

To investigate the failure mechanism and the effects of in-situ load condition on the remaining burst strength of corroded casing, advanced FEA was performed for the 20 burst test specimens. Analyses were conducted under both capped-end condition and the in-situ downhole load condition with locked-in axial load/strain. Analysis results under the capped-end condition were calibrated with the physical burst test data to establish the appropriate failure criterion for predicting the burst strength. Additional analyses were then performed under the in-situ load condition to investigate the impact of axial constraint provided by the well cement on casing burst strength.

3.1. Model Description

FEA models of the casing burst test specimens were generated using the commercial FEA program Abaqus v2020 [13]. The detailed geometrical profiles of the metal-loss features were captured by laser scan to generate the FEA models. Three-dimensional 20-node quadratic brick elements (C3D20R) were used. The mesh size within the local metal-loss region was in the range of approximately 0.5 to 1 mm (0.02 to 0.04 in). In addition, the local metal-loss region was meshed with four layers of elements along the thickness direction to capture the local through-wall non-uniform stress and strain distributions. Mesh sensitivity analysis was performed to ensure the mesh density was sufficient to produce converged results. Figure 6 shows an example of the FEA model of a 114.3 mm (4.5 in) casing with a metal-loss feature.

Using the stress-strain curves from the coupon tensile tests, the J55 casing material models were developed with an elastic-plastic constitutive relationship and an isotropic hardening rule. The von Mises yield criterion and associated flow rule were used. Since converting the engineering stress-strain curve to the true stress-strain curve becomes invalid after the coupon necking point (i.e., at the UTS), no further strain hardening was considered beyond the UTS point. Geometric non-linearity was enabled in all analyses.

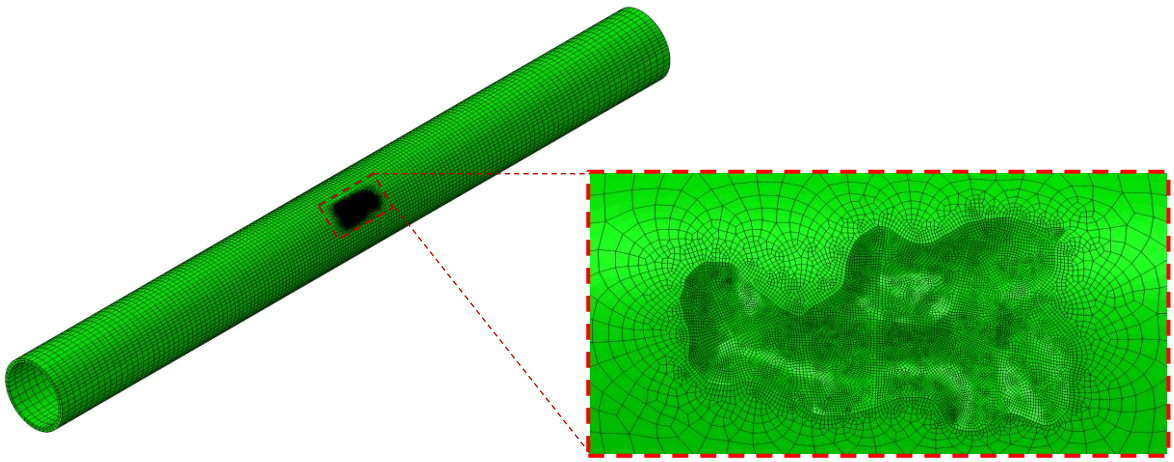

Figure 6 – Casing specimen FEA model mesh example

3.2. Load Conditions

In the capped-end load analysis, two hemispherical end caps were attached on both ends of the casing model. Under the capped-end condition with pure internal pressure load scenario, the axial stress (σ_1) and hoop stress (σ_2) in a thin-wall pipe body can be approximated by Eq. 1 and Eq. 2, respectively.

$$\sigma_1 \approx \frac{P\pi D^2/4}{\pi D t} = \frac{PD}{4t} \quad (1)$$

$$\sigma_2 \approx \frac{PD}{2t} \quad (2)$$

where D is the pipe outside diameter (OD), t is the pipe wall thickness (WT), and P is the internal pressure. Therefore, the stress ratio between the axial and hoop components is approximate 0.5.

However, the casing stresses in a well can be significantly different from the capped-end condition. Well construction imposes various loads on the casing string, such as the hanging weight, buoyancy force, and bending load induced by the wellbore curvature. These forces imposed on the casing string during installation and cementing are generally "locked-in" to the string once the cement is set and cured. Since additional stress components induced by these in-situ loads will affect the onset of yielding and post-yield response of the casing materials, it is expected that these in-situ casing loads would also affect the burst strength of the casing. Based on the load and boundary conditions that are reasonably representative of the downhole conditions in a UGS well, two extreme scenarios were considered in this study [2]:

- Maximum locked-in axial compressive strain (approximately -0.050% to -0.058%) at the bottom of the well; and
- Maximum locked-in axial tensile strain (approximately 0.010% to 0.015%) at the top of the well.

The in-situ load analysis was performed in two steps. In the first step, the initial axial strain was applied to the casing model, and the model was allowed to deform radially and circumferentially. In the second step, an internal pressure was gradually applied on the inner surface of the casing, while both ends of the model were axially constrained to simulate the in-situ cement confinement condition. For conservatism, the potential benefit of cement radial confinement to casing burst strength was not considered in the analysis. The generalized Hooke's law establishes the relationship between the axial strain and the three principal stress components in the pipe body. An incremental form of this relationship can be expressed by Eq. 3:

$$\dot{\varepsilon_a} = \frac{1}{E}[\dot{\sigma_a} - v(\dot{\sigma_h} + \dot{\sigma_r})] \quad (3)$$

where

$\dot{\varepsilon_a}$ is the axial strain increment,
$\dot{\sigma_a}$ is the axial stress increment,
$\dot{\sigma_h}$ is the hoop stress increment,
$\dot{\sigma_r}$ is the radial stress increment,
E is the Young's modulus, and
v is the Poisson's ratio.

For a thin-wall pipe, the radial stress component ($\dot{\sigma_r}$) is much smaller than the axial and hoop stress components. Therefore, in an axially constrained pipe ($\dot{\varepsilon_a} = 0$), the ratio between $\dot{\sigma_a}$ and $\dot{\sigma_h}$ is approximately equal to v (~0.3 for steel).

3.3. Failure Criterion

Predicting the burst pressure of a pipe with FEA requires an appropriate failure criterion. In general, two types of failure criteria have been commonly used to predict burst pressure of both corroded and uncorroded pipes. With this project providing both detailed metal-loss profiles and accurate stress-strain relationship in the FEA model, all information was available to validate the failure criterion and to investigate the failure mechanism of burst failure of corroded pipe.

3.3.1. von Mises Equivalent Stress Criterion

Many previous studies that used FEA to predict burst pressure of corroded pipes have used failure criteria that associate the von Mises Equivalent stress (VME) in the corroded ligament (i.e., remaining pipe wall in a corrosion feature) with the material's true tensile strength [4,14,15]. Slight variations of the criteria were used in these studies, such as using the minimum, maximum, or average value of the VME. The criterion adopted by BS 7910 Annex G [16] suggests that burst may be considered to occur when the average VME through the minimum ligament of the metal-loss area equals the material's true tensile strength.

3.3.2. Plastic Collapse Criterion

Another failure criterion is defined as the maximum load where local structural instability occurs due to large plastic deformation, which is usually referred to as plastic collapse or plastic instability. For a pipe under internal pressure load, local plastic collapse failure occurs when the rate of pipe cross-section geometry change (i.e., diameter increase and wall thinning) induced by plastic deformation exceeds the rate of material strain hardening. Numerical methods, such as the "Riks" method in Abaqus, are often used to determine the maximum load capacity for structural instability problems. This approach has been used to predict the burst capacity of uncorroded line pipe [17] and corroded line pipe [18].

3.3.3. Failure Criterion Assessment

Both failure criteria described above were used to predict the burst pressure under the capped-end condition. Note that, when using the VME criterion, the maximum VME through the minimum ligament of the metal-loss area was considered by following the approach used by Chauhan et al. [4]. Figure 7 shows an example of the relationship between the internal pressure and the equivalent plastic strain within the critical remaining ligament of the metal-loss feature shown in Figure 6. The plastic collapse criterion resulted in a predicted burst (peak) pressure of 43.77 MPa (6,348 psi) at

~55% plastic strain, which is quite close to the actual test result of 43.89 MPa (6,366 psi). The VME criterion resulted in a burst pressure of 33.78 MPa (4,899 psi) at ~7.4% plastic strain, which is only 77% of the measured burst pressure.

A summary of the predicted burst pressure for all 20 burst specimens using the two criteria is plotted in Figure 8. The prediction capability between the two criteria was quantitatively evaluated using the ratio of the predicted versus actual burst pressure (referred to as the "predicted-to-actual pressure ratio" or "prediction ratio" in the following text). A ratio equal to one indicates a perfect prediction and any deviation from one represents the model error. For each set of FEA results, the prediction ratio was determined for all 20 test cases. In addition, a mean value and a coefficient of variation (COV) were determined for each set of prediction ratios. The difference between the mean value and one represents the bias error of the prediction. The COV represents the ratio of the standard deviation to the mean and is a measure of the scatter and reflects the level of random error of the prediction. Therefore, the best prediction should have a mean prediction ratio closest to one and the lowest COV. The bias error of the prediction can be corrected by applying a multiplicative factor calibrated with a statistically significant number of tests. However, the random error cannot be removed, and it is a critical measure of the model's prediction capability.

The VME criterion was found to significantly under-estimate the burst pressure, which is reflected by a low prediction ratio mean of 0.886. The plastic collapse criterion was found to slightly over-estimate the burst pressure, but with a much better prediction ratio mean of 1.017. Additional evidence in the literature regarding the prediction performance of the two criteria in FEA were also identified in a previous PHMSA-sponsored project [18]. In fact, there has been a long history of applying the plastic collapse (instability) criterion in analytical models for predicting the ductile rupture strength of uncorroded pipes [19,20,21,22,23]. This study provides strong evidence that ductile burst of corroded pipe shares the same fundamental physics as that of uncorroded pipe. Therefore, prediction of ductile burst of corroded pipe should use the plastic collapse or plastic instability criterion.

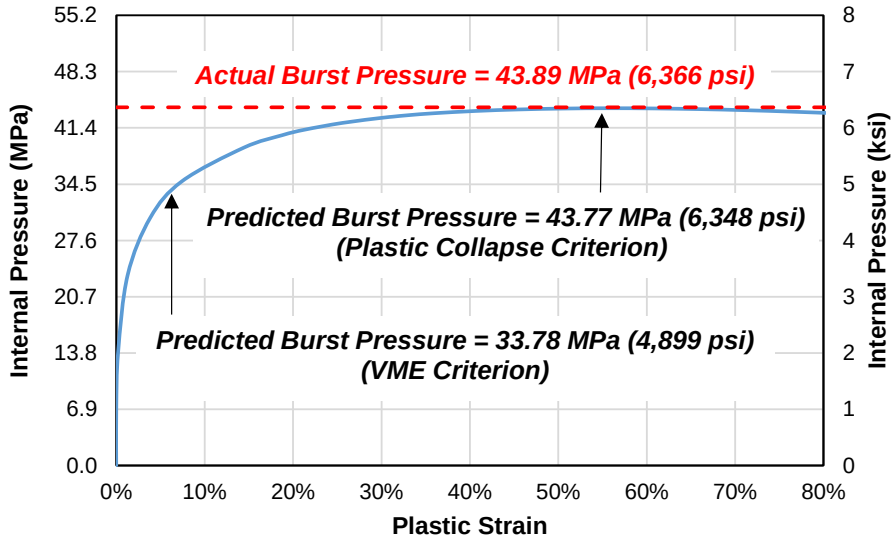

Figure 7 – Prediction of burst pressure using FEA

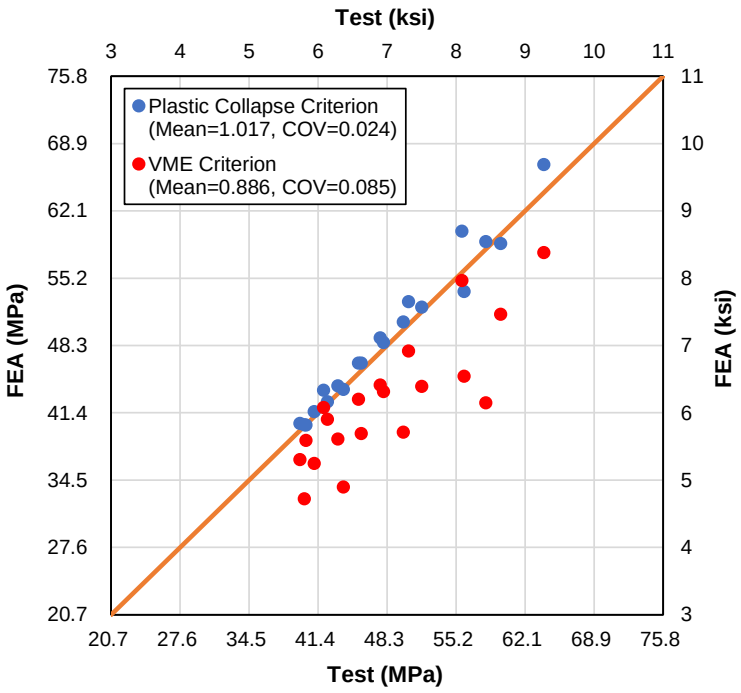

Figure 8 – Comparison of FEA prediction using different failure criteria

Figure 9 shows the equivalent plastic strain distribution within the metal-loss region at the peak pressure for the example feature shown in Figure 6. The plastic strain plot clearly shows the initiation of local necking along the large plastic strain band, indicated by the red color. An excellent agreement was found between the predicted necking zone and the actual rupture region in the failure specimen (see the left picture in Figure 5). The excellent agreement between the FEA prediction and the physical burst test for the failure location (leak or rupture) was found in 19 of the 20 burst specimens. The one exception could likely be due to local variations in material properties or inaccuracies in the modeled metal-loss profile. All full-scale burst test specimens showed signs of necking and/or significant plastic deformation at the failure location, which confirms the ductile plastic failure mode.

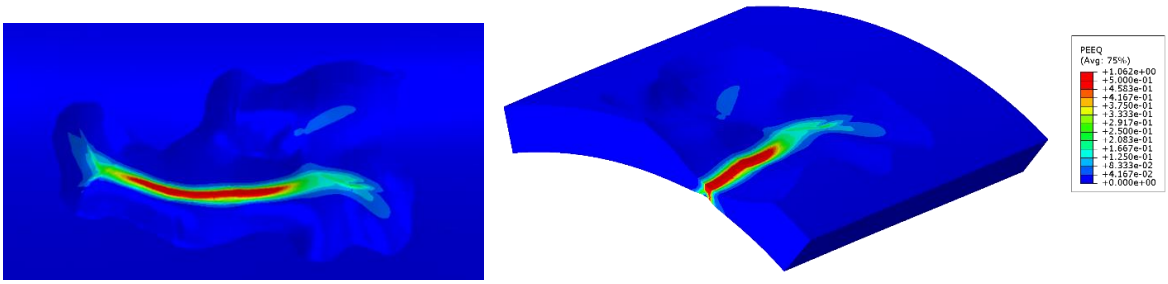

Figure 9 – Equivalent plastic strain distribution at peak pressure

3.4. Effects of Locked-in Axial Loads

The effects of the locked-in axial loads on the remaining burst strength were statistically evaluated using the mean and COV of the ratios of the FEA-predicted pressures between the in-situ load scenario and the capped-end scenario. The maximum locked-in compression was found to result in a marginal reduction of the burst strength compared to the capped-end condition (mean = 0.983 and COV = 0.010), while the maximum locked-in initial tension was found to have a negligible impact on the burst strength (mean = 1.002 and COV = 0.002).

A similar finding was also reported in a previous PHMSA-sponsored project by Liu et al. [18]. Their study was based on FEA and full-scale burst tests of corroded line pipe under very high compressive strain (up to 2.3%). The results showed that the burst pressure reduction due to longitudinal compressive strain was small. In addition, the study also indicated that axial compressive strain has a greater influence on the burst pressure of specimens with longitudinal grooves than those with other types of metal-loss features.

To better understand the phenomenon, a further investigation was undertaken to examine the stress condition within the metal-loss region under different load scenarios. Figure 10 shows an example of the two primary stress components (axial and hoop) at a critical location within the necking region of the metal-loss feature shown in Figure 6. Note that the radial stress and the three shear stress components were found to be about an order of magnitude smaller than the two primary stress components and, therefore, are not considered in this discussion. The analysis results at the same location for the three load scenarios (capped-end, fixed axial strain with pre-tension, and pre-compression) are included in the same chart for comparison. The three key material parameters, i.e., the proportional limit, the API yield strength (YS), and the UTS, are plotted with VME envelopes as references to illustrate the boundaries between the elastic, elastic-plastic transition, and large plastic deformation regions. At the peak pressure, the pipe body stress exceeded the proportional limit in all three cases. Since the incremental plastic strain between the proportional limit and the API YS is relatively small (see Figure 2), the slope of the stress paths in the pipe body stayed relatively constant (i.e., an axial versus hoop stress ratio of 0.5 for the capped-end condition and 0.3 for the axially constrained condition). However, the stress paths in this particular metal-loss feature in all three cases followed an initial slope close to that in the axially constrained condition within the elastic region, and finally converged to the stress path under the capped-end condition (i.e., an axial versus hoop stress ratio of 0.5).

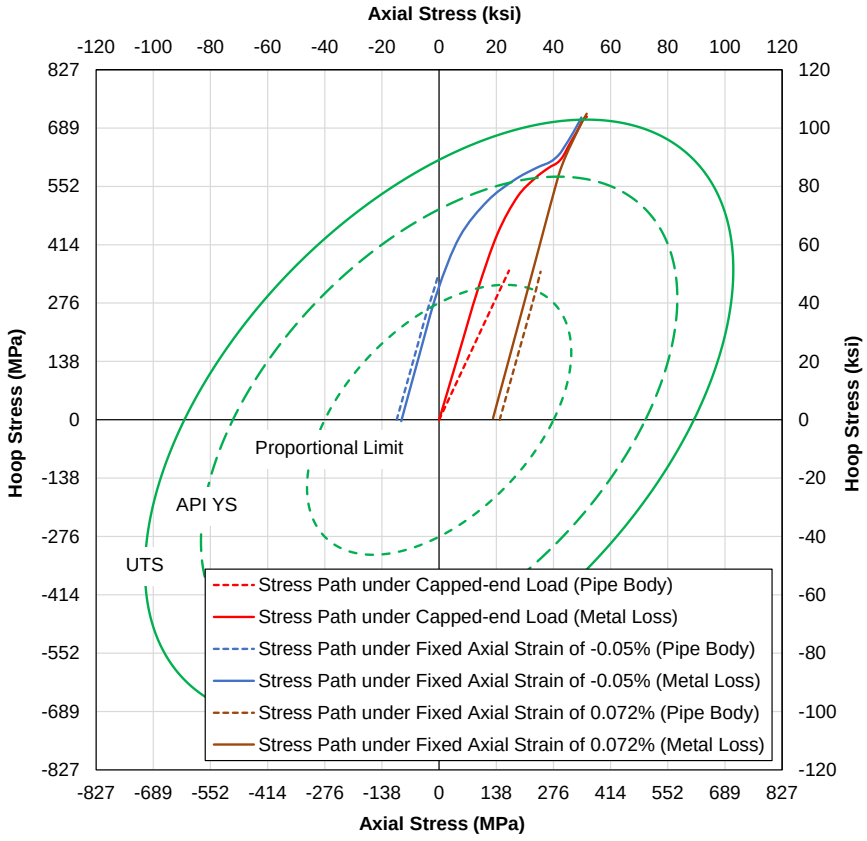

Figure 10 – Stress paths in the metal-loss region in burst analysis of a metal-loss feature

Under the axially constrained condition, the deviation of the stress path after the onset of yielding and its convergence towards the final capped-end stress path are driven by the plastic deformation following the associated flow rule and can be demonstrated by classical elasticity and plasticity theories. In all three cases, the local metal-loss region is constrained by the more rigid surrounding pipe body, which affects the axial stress transferred from the pipe body into the metal-loss region. Therefore, the initial slope of the stress path (i.e., within the elastic range) within the metal-loss region does not necessarily follow that in the uncorroded pipe body, and it is highly dependent on the local metal-loss geometry and the constraint condition from the surrounding pipe body. After yielding of the metal-loss region, the stress and strain within this region become less dependent from the load condition in the surrounding uncorroded pipe. Therefore, further evolution of the stress and strain associated with large plastic deformation within the metal-loss largely follow an axially constrained condition, which finally converges to the stress path under the capped-end condition. Similar behavior of the local stress path convergence within the metal-loss feature was also observed in all other cases.

The convergence of the stress path after the elastic-plastic transition led to similar stress and strain states in the different load scenarios examined in this study. Since the plastic strain development within the elastic-plastic transition region is relatively small, the effect of path dependency on the final plastic collapse (which occurs at a much higher plastic strain level) is small. Therefore, this explains the similar predicted burst pressure in the different load scenarios in this FEA study. Further discussion of this behavior and the small effect of pre-strains on the ductile rupture strength of uncorroded pipe is described by Stewart et al. [22].

Note that some existing methods (e.g., API 579-1 level 2 model [24], BS 7910 model [16], and DNVGL-RP-F101 model [25]), to account for axial load effects, assume a linear relationship between the axial stress in the metal-loss region and the pipe body. However, the investigation of the local stress response within the metal-loss region suggests that this assumption is not valid in these cases, especially after the onset of yielding. Therefore, further study including additional FEA and full-scale validation tests is warranted to gain a better understanding of the in-situ load impact and to improve the methodology to account for such in-situ load effects in predicting the remaining burst strength.

4. MODEL BENCHMARK

The majority of popular remaining burst strength prediction models share the general form of the equation shown in Eq. 4.

$$S_F = S_{flow} \frac{1-\frac{A}{A_0}}{1-\frac{1}{M}\left(\frac{A}{A_0}\right)} \tag{4}$$

where

S_F is the nominal pipe body hoop stress limit at failure,
S_{flow} is the flow stress as a function of yield strength and/or ultimate strength,
A is the cross-sectional area of the metal-loss,
A_0 is the nominal cross-sectional area of the pipe wall, and
M is the Folias factor to account for the bulging effect at the metal-loss location.

Eq. 4 reflects the impact of the metal-loss on the nominal hoop stress limit at failure. The relationship between the internal pressure and the nominal pipe hoop stress is based on Barlow's equation (Eq. 5), where P_F is the failure pressure and t is the pipe wall thickness. The different methods use either the nominal OD or mid-wall diameter for the parameter D in the burst prediction model.

$$P_F = \frac{2S_F}{D/t} \quad (5)$$

Note that these methods assume the ductile failure mode and are only applicable when the following conditions are satisfied:

- The metal-loss features are blunt (i.e., no crack-like elements) and the material is fully ductile;
- The primary load is internal pressure, while other loads, such as axial tension/compression, bending, external pressure, and shear, are relatively insignificant;
- The pipe has no significant cross-sectional deformation, such as dents, which may cause a significant change in the stress distribution compared to a non-deformed pipe; and
- The maximum metal-loss depth does not exceed approximately 80% to 85% of the nominal WT.

The full-scale burst test results were used to evaluate the predictive capability of eight commonly used remaining burst strength analytical models that have been previously developed in the pipeline and petrochemical industries. Actual YS and UTS obtained from the coupon tests were used instead of the specified minimum yield strength and SMTS in the model calculation. Note that API 579-1 does not provide a definition of the flow stress. In this study, the average between the actual YS and UTS was used as the flow stress in the API 579-1 prediction, which was found to provide the best prediction against test data by Francini et al. [5]. Figure 11 shows the comparison between the predicted and actual burst pressure values for the eight prediction models.

Using the approach described above in evaluating the FEA failure criteria, the analytical model prediction capability was quantitatively evaluated using the predicted-to-actual pressure ratio (the "prediction ratio"). The mean and COV of the prediction ratio of all models are presented in Figures 12 and 13. Comparing the mean and COV values of the prediction ratio for all models led to the following observations:

- All analytical models under-estimate the remaining burst strength by approximately 10% to 36%, as indicated by the mean predicted-to-actual pressure ratio;
- The CSA model [26] showed the smallest bias error among the eight analytical models, with an average under-estimation of ~10%;
- The RSTRENG model showed the lowest COV. However, this model is currently difficult to use for downhole casing as it requires accurate river bottom profiles of metal-loss features, which are beyond the capability of the current downhole casing corrosion inspection technologies;
- Excluding the RSTRENG model, which is difficult to use for downhole casing, the ASME B31G and modified B31G models [27] showed the lowest random error (COV);
- The API 579-1 model showed both the largest bias error (i.e., lowest mean) and random error (i.e., largest COV); and
- Since the LPC-1, BS 7910, and the DNVGL-RP-F101 models share similar forms of equations, they showed similar random errors. The difference in the bias error among the three models resulted from the different flow stress definitions used.

It must be emphasized that the observations were based on only 20 burst tests with limited metal-loss profiles and a single casing grade (J55). Additional test data of a broader range of metal-loss profiles and casing grades are needed to better understand the model prediction capabilities and to draw reliable conclusions.

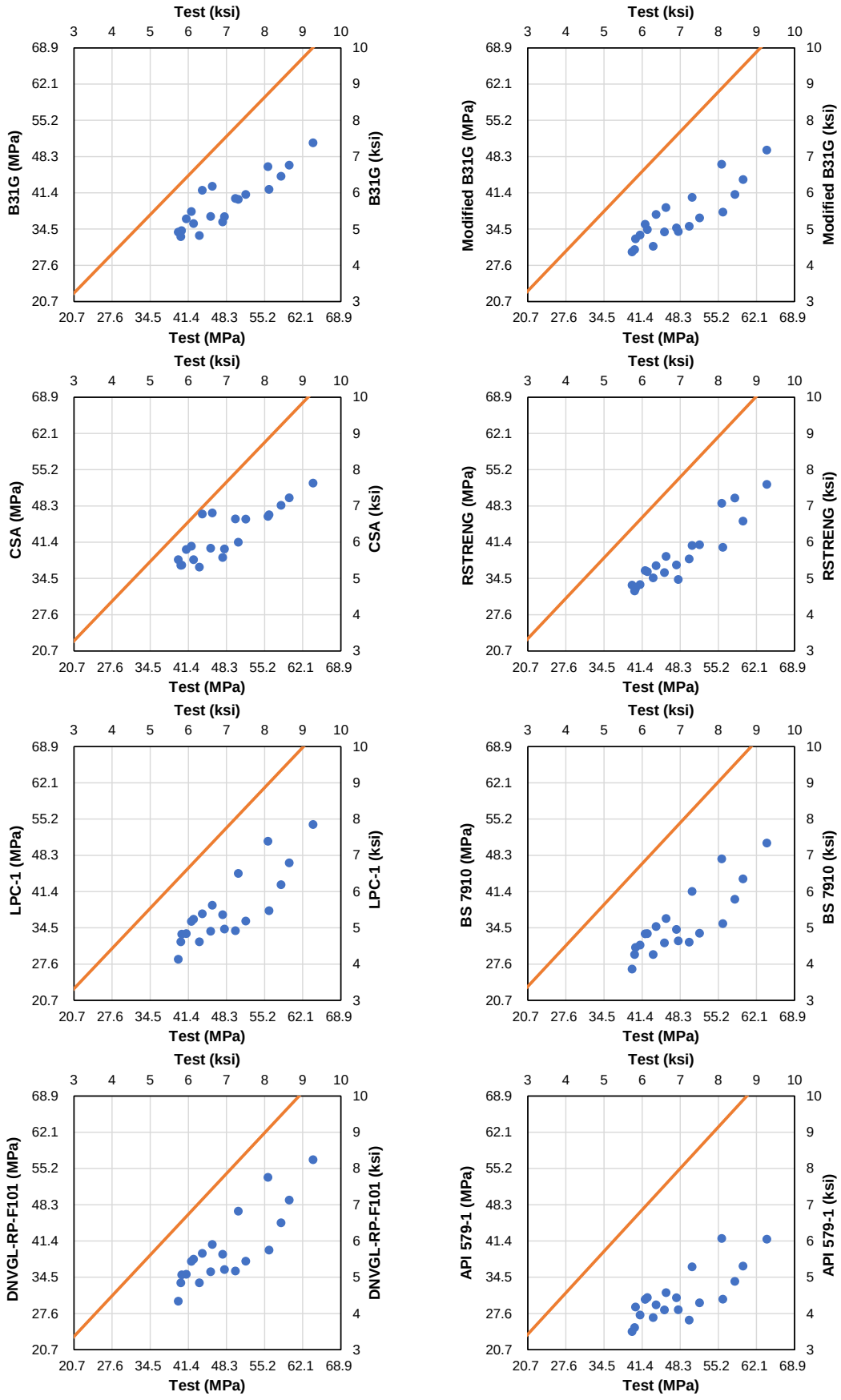

Figure 11 – Benchmark of remaining burst strength prediction models

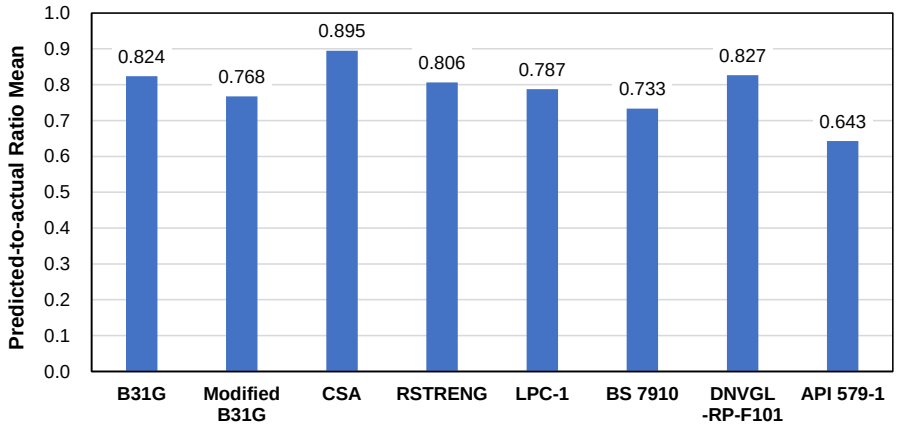

Figure 12 – Mean value of the predicted-to-actual pressure ratio

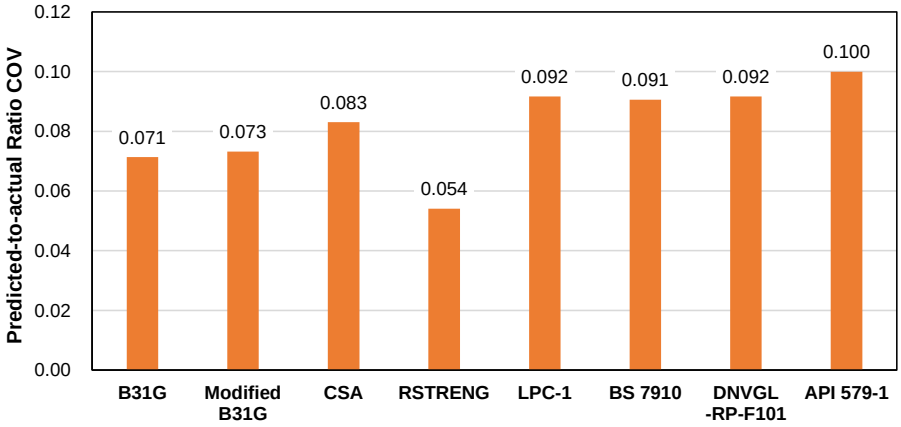

Figure 13 – COV of the predicted-to-actual pressure ratio

Note that the majority of these analytical remaining burst strength prediction models were developed based on extensive burst test datasets of line pipe samples that had D/t ratios exceeding 40 [3], whereas the casing specimens in this study ranged from 18 to 22.1. A careful review of these remaining burst strength prediction models indicates that the non-dimensional parameter $L/\sqrt{Dt}$ in various forms of the Folias factor can be re-formulated as $(L/t)/\sqrt{D/t}$. The component L/t is the ratio between the metal-loss feature length and the pipe WT, and it reflects the geometric characteristic of the feature. On the other hand, the factor of the D/t ratio is implicitly included in the Folias factor. Therefore, the form of the Folias factor directly affects the burst pressure model prediction capability for pipes with different D/t ratios. As a result, it is likely that the Folias factors calibrated based on large D/t line pipe samples are not suitable for small D/t casing samples. Further study is required to adjust the Folias factor for downhole casing geometries to improve the analytical model prediction accuracy.

In addition, this study identified that the ductile burst of corroded casing is dominated by the plastic instability failure mechanism, which depends on both local pipe geometry and the post-yield stress-strain relationship, which is often formulated using the UTS and a strain hardening index. Therefore, considering the post-yield strain hardening property in remaining burst strength prediction models is expected to improve the model accuracy. A recent review conducted by Zhu [28] shows a few new

generation models that explicitly included the strain hardening index. Further assessment of the performance of these models is highly recommended.

5. CONCLUSIONS AND RECOMMENDATIONS

This paper summarizes the findings of a comprehensive study that evaluated the prediction capability of various remaining burst strength models for downhole casing applications. This investigation involved full-scale burst tests, FEA, and model benchmarking using 20 casing specimens with a variety of metal-loss features. The following key findings were identified and are expected to have a significant influence in further development of remaining burst strength prediction models, not only for application in downhole casing, but also pipeline and other industries:

- Every remaining burst strength model evaluated under-estimates the burst capacity of corroded casing. The pipe D/t parameter implicitly included in the Folias factor is likely the cause, since models calibrated based on large D/t line pipe samples are not suitable for smaller D/t casing samples.
- The comparison between FEA and full-scale burst tests provided strong evidence of the plastic instability failure mechanism for the failed specimens. Therefore, FEA prediction of remaining burst should use a criterion based on plastic collapse (instability) rather than on VME. In addition, since plastic instability is dependent on material strain hardening behavior, consideration of the strain hardening behavior is expected to improve the remaining burst strength prediction models.
- Downhole in-situ locked-in axial loads were found to have a marginal impact on the remaining burst strength of casing. Assumptions used in some existing methods to account for axial load effects on remaining burst strength were shown to be invalid, and further investigation is needed to account for these loads.
- The casing material showed time-dependent stress-strain response in the post-yield region in the coupon test at room temperature. Therefore, the casing burst strength obtained from laboratory tests (under a relatively high strain rate) would over-estimate the actual burst strength in the well (under a relatively low strain rate or sustained pressure). If left untreated in the calibrated models, this can pose a hidden threat to the casing integrity.

Based on the outcomes of this study, the following recommendations are made for future work:

- Additional full-scale burst tests should be conducted on downhole casing samples to expand the test dataset to support model improvement with the following considerations:
  - Include additional metal-loss profiles that cover a broad range of casing corrosion conditions;
  - Include additional casing sizes and weights to investigate the D/t ratio effect;
  - Include additional casing grades (e.g., K55, N80, L80, P110) to support development of advanced models considering material strain hardening properties; and
  - Upon further validation of FEA models with additional test results, use FEA to supplement physical tests for the purposes of reducing cost and investigating the effects of complex loading conditions on remaining burst strength.
- Further investigation of in-situ locked-in axial load effects on casing remaining burst strength should be conducted with full-scale burst tests and FEA to develop an appropriate method to account for such effects.
- Additional study is required to understand the mechanical properties and the burst failure behavior of vintage casing in existing UGS wells, as around 80% of UGS wells were drilled before 1980 [29]. Special attention should be paid to the ductility of vintage casing materials and their burst failure mode (i.e., ductile versus brittle), which could have a significant impact on the prediction capability of existing remaining burst strength prediction models.
- The strain rate effect on remaining burst strength of corroded casing should be investigated to properly account for the sustained downhole pressure condition.

6. ACKNOWLEDGEMENT

The authors sincerely acknowledge and appreciate the financial support from PHMSA and PRCI, as well as the technical advice provided by the members of the Underground Storage Technical Committee at PRCI. Special thanks are also extended to Ms. Zoe Shall (Senior Program Manager, Integrity & Inspection and Underground Storage at PRCI) for the direction and oversight provided throughout the execution of this research program.

7. REFERENCES

1. Tao G (2019). *Casing corrosion logging tool test OR-244-16704-R01*. Chantilly, VA: Pipeline Research Council.
2. Tao G and Stephens M (2021). *Evaluation of casing integrity for underground storage wells PR-244-18702-R01*. Chantilly, VA: Pipeline Research Council.
3. Chauhan V and Brister J (2009). *A review of methods for assessing the remaining strength of corroded pipelines*. Loughborough, UK: GL Industrial Services UK.
4. Chauhan V, Grant R and Wood A (2004). *Well bore integrity – development of methods for assessing corrosion metal loss defects in casing strings GRI-05/0171.* Des Plains, IL: Gas Research Institute.
5. Francini RB, Wahl JD and Zelenak PA (2008). *Effects of tensile loading on the remaining strength of corroded casing DE-FC26-03NT41779.* Worthington, OH: Kiefner and Associates.
6. Francini RB and Quade NT (2010). *Extension of a method to validate the remaining strength of corroded casing to additional cases DE-FC26-03NT41779.* Worthington, OH: Kiefner and Associates.
7. ASTM E111-17: *Standard test method for Young's modulus*. ASTM International, 2017.
8. ASTM A370-20: *Standard test methods and definitions for mechanical testing of steel products*. ASTM International, 2020.
9. ASTM E8/E8M-16A: *Standard test methods for tension testing of metallic materials.* ASTM International, 2016.
10. API 5CT 10th Edition: *Casing and tubing*. American Petroleum Institute, 2018.
11. Tao G, Matthews C and Adams A (2020). *Special considerations for well tubular design at elevated temperatures*. SPE Drilling and Completions, SPE 199570-PA.
12. API 5C3 7th Edition: *Calculating performance properties of pipe used as casing or tubing.* American Petroleum Institute, 2018.
13. Dassault Systemes (2020). *SIMULIA User Assistance*. Paris: Dassault Systemes.
14. Liu J, Chauhan V, Ng P, Wheat S and Hughes C (2009). *Remaining strength of corroded pipe under secondary (biaxial) loading R9068*. Loughborough, UK: GL Industrial Services UK.
15. Bao J, Zhang S, Zhou W and Zhou S (2018). *Evaluation of burst pressure of corroded pipe segments using three-dimensional finite element analyses IPC2018-78130.* International Pipeline Conference 2018, Calgary, Alberta, ASME, New York.
16. BS 7910:2019: *Guide to methods for assessing the acceptability of flaws in metallic structures*. British Standards Institution, 2019.
17. Zhu X and Leis BN (2006). *Theoretical and numerical predictions of burst pressure of pipelines PVP2006-ICPTV-11.* ASME Pressure Vessels and Piping Division Conference 2006, ASME, New York.
18. Liu M, Zhou H, Wang B and Wang Y (2017). *Strain-based design and assessment in critical areas of pipeline systems with realistic anomalies DTPH56-14-H-00003.* Washington, DC: Pipeline and Hazardous Materials Safety Administration.
19. Swift HW (1952). *Plastic instability under plane stress*. Journal of Mechanics and Physics of Solids, 1(1), pp. 1-18.
20. Mellor PB (1962). *Tensile instability in thin-walled tubes.* Journal of Mechanical Engineering Science, 4(3), pp. 251-256.

21. Chakrabarty J and Alexander JM (1969). *Plastic instability of thick-walled tubes with closed ends.* International Journal of Mechanical Sciences, 1192), pp. 175-186.
22. Stewart G, Klever FJ and Ritchie D (1994). *An analytical model to predict the burst capacity of pipelines.* Pipeline Technology, v, pp. 177-188.
23. Zhu X and Leis BN (2012). *Evaluation of burst pressure prediction models for line pipes.* International Journal of Pressure Vessels and Piping, 89, pp. 85-97.
24. API 579-1/ASME FFS-1: *Fitness-for-service*. American Petroleum Institute, 2016.
25. DNVGL-RP-F101: *Corroded pipelines*. DNV GL AS, 2019.
26. CSA Z662:19: *Oil and gas pipeline systems*. CSA Group, 2019.
27. ASME B31G-2012: *Manual for determining the remaining strength of corroded pipelines: supplement to ASME B31 code for pressure piping*. American Society of Mechanical Engineers, 2012.
28. Zhu X (2021). *A comparative study of burst failure models for assessing remaining strength of corroded pipelines.* Journal of Pipeline Science and Engineering, 1, pp. 36-50.
29. US Department of Energy (2016). *Ensuring safe and reliable underground natural gas storage.* https://www.energy.gov/downloads/report-ensuring-safe-and-reliable-underground-natural-gas-storage.